Melting of quasi-two-dimensional crystalline Pb supported on liquid Ga

Dongxu Li and Stuart A. Rice
Department of Chemistry and The James Franck Institute, The University of Chicago, Chicago, Illinois 60637, USA
(Received 14 June 2005; published 20 October 2005)

Experimental studies have shown that the Pb monolayer that segregates in the PbGa alloy liquid-vapor interface forms a two-dimensional hexagonal crystal that melts at 341 K, and it has been speculated that the disordered phase formed is hexatic. This paper reports the results of simulation studies of the in-plane structure of the outermost stratum of the liquid-vapor interface of a dilute Pb in Ga alloy. These simulations are based on four major improvements to a previous study. First, the simulation studies involve considerably more atoms and considerably longer equilibration runs than considered in the previous work of Chekmarev, Oxtoby, and Rice. Second, a more accurate nonlocal pseudopotential representation of the interactions in the system is used. Third, the amplitude of the out-of-plane motion of the Pb atoms is constructed to have the observed value. Fourth, an approximation to the role of the liquid Ga substrate is provided by adding a layer of Ga atoms to the layer of Pb atoms. The results of our simulation studies show that the Ga layer adjacent to the Pb layer has a profound influence on that layer's properties. In particular, it is shown that in the two-layer PbGa system the Pb layer forms, at low temperature, a stable two-dimensional crystal on top of liquid Ga. This two-dimensional crystal melts at a temperature close to that found experimentally. It is found that the crystalline Pb layer is transformed to the liquid state via two intermediate hexatic phases that differ in the magnitude of the bond orientation order. Each of the phase transitions along this melting pathway is first order. The temperature range over which each hexatic phase is stable is small. The profound influence of out-of-plane motion is demonstrated by a comparison of the results of simulations of a quasi-two-dimensional (Q2D) and of a strictly two-dimensional monolayer of Pb. The melting transition in the Q2D one-layer system is first order, directly to the liquid, with no intervention of a hexatic phase. The melting transition in the strictly 2D system involves two stages: a first-order transition to an intermediate hexatic phase followed by melting of the hexatic to a liquid phase. The latter transition is continuous over a small temperature range. An examination of the role of defects in the melting process reveals a picture rather different from that postulated in the Kosterlitz-Thouless-Halperin-Nelson-Young theory of 2D melting.

DOI: 10.1103/PhysRevE.72.041506 PACS number(s): 64.70.Dv, 68.03.−g

I. INTRODUCTION

Recent experimental studies of the structure of the liquid-vapor interface of a dilute Pb in Ga alloy reveal, as expected, that the excess Pb in the interface is present as a monolayer that forms its outermost stratum [1]. Since the Pb monolayer has a nonzero amplitude of motion perpendicular to the interface, we characterize it as quasi two dimensional (Q2D). These experiments also reveal, unexpectedly, that when the temperature is below 341 K the Pb monolayer is in a Q2D hexagonal crystalline phase and that at 341 K it undergoes a transition, with either very small or zero density change, to a disordered phase. The correlation length obtained from the width of the (1,1) diffraction peak of the Q2D crystalline phase drops almost discontinuously at 341 K to a value rather larger than is typical of liquids. It then further decreases continuously until about 363 K, thereafter becoming constant. These data suggest the existence of a disordered phase in the temperature range 341–363 K, intermediate between the crystal phase and the liquid phase. The experimental data fall short of providing unambiguous evidence for the existence and character of this intermediate disordered phase, but it has been speculated that it has a hexatic structure. The disordered phase that is stable above 363 K is a Q2D liquid. Second-harmonic generation studies of the liquid-vapor interface of PbGa alloys have been interpreted to confirm the crystallization of a monolayer of Pb in the liquid-vapor interface, albeit at a temperature slightly different (357–362 K) from that found in the grazing-incidence x-ray diffraction studies. Elsewhere we have argued that the second-harmonic generation studies identify the liquid-to-hexatic transition [2].

Information about the atomic distribution in the liquid-vapor interface of a dilute Pb in Ga alloy has also been obtained from self-consistent quantum Monte Carlo simulations [3]. The sample is constructed with enough layers of atoms that in its interior the properties of the bulk liquid are correctly reproduced. The results of the studies of a 1000-atom sample of a dilute Pb in Ga alloy, arranged in 14 layers with two liquid-vapor interfaces, reported by Zhao and Rice [3], accurately describe the longitudinal (along the normal to the interface) density distributions of the Pb and Ga atoms, but they do not describe correctly the in-plane distribution of the atoms in the Pb monolayer. This failure is plausibly attributable to the inadequate size of the interface (about 70 atoms) in the simulation sample used. The surface area of the Zhao-Rice simulation [3] sample is adequate for characterization of the short-ranged in-plane structure of a liquid, but not the long-ranged in-plane structure of a solid.

In the limiting case when the monolayer-substrate interaction is very weak it is plausible to analyze the properties of the segregated species in the outermost layer of the liquid-vapor interface as if isolated from the substrate alloy. The

calculations of Zhao and Rice [3] show that the Pb-Pb interaction is much stronger than the Ga-Ga and Pb-Ga interactions, which led Chekmarev, Oxtoby, and Rice (COR) [4] to study the properties of a Q2D sheet of Pb atoms. The results of their calculations reproduce qualitatively all of the major features of the Pb-in-Ga system observed experimentally. These simulations also predict the existence of a hexatic phase, stable over a very small range of temperature, between the Q2D crystal and Q2D liquid phases. However, the size of the simulation sample used in the COR calculations was only 2000 atoms, which is not large enough to guarantee that finite-size effects did not influence the findings, specifically whether the hexatic phase is an artifact of system size or will persist in the thermodynamic limit. Moreover, those calculations used a rather simple local pseudopotential and a crude constraint on the out-of-plane motion of the Pb atoms. A consequence of the choice of pseudopotential and out-of-plane potentials is that the temperature scale of the phase diagram is shifted up considerably; COR predict the melting point of the ordered quasi-two-dimensional solid to be of the order of 1300 K. As the simulations reported in this paper show, the melting point of the Pb monolayer depends sensitively on the magnitude of the out-of-plane motion of the Pb atoms. The use of experimental data to determine the magnitude of the out-of-plane motion removes the gross discrepancy in the magnitude of the transition temperature predicted. The simulations reported in this paper also show that the Ga layer adjacent to the Pb layer has a profound influence on that layer's properties, including the existence or nonexistence of a hexatic phase. As will be seen, our results require a reinterpretation of the results of Chekmarev, Oxtoby, and Rice.

This paper reports the results of simulation studies of the in-plane structure of the outermost stratum of the liquid-vapor interface of a dilute Pb in Ga alloy. These calculations examine model systems that have four major improvements relative to the model used in the COR simulations. First, the simulations reported in this paper involve considerably more atoms and considerably longer equilibration runs than considered by Chekmarev, Oxtoby, and Rice [4]. Second, a more accurate pseudopotential representation of the interactions in the system is used. Third, the amplitude of the out-of-plane motion is constructed to have the observed value (taken from the fit to the x-ray reflectivity data for the PbGa alloy). Fourth, instead of neglecting the influence of the substrate Ga on the properties of the Pb monolayer, an approximation to the role of the liquid Ga substrate is provided by adding a layer of Ga atoms to the layer of Pb atoms. As already mentioned, the results of our simulation studies show that the Ga layer adjacent to the Pb layer has a profound influence on that layer's properties. In particular, it is shown that a monolayer of Pb that has atomic out-of-plane motion with amplitude equal to the observed value forms a two-dimensional crystal that melts to a liquid via a first-order transition; this model does not support a hexatic phase intermediate between the crystal and liquid phases. On the other hand, it is found that in the model two-layer PbGa system the Pb layer forms, at low temperature, a stable two-dimensional crystal on top of liquid Ga that melts to a hexatic phase via a first-order transition and then, at a higher temperature, via another first-order transition, to another hexatic phase, before finally transforming to a liquid. The crystal-to-hexatic transition temperature is close to that found experimentally. The temperature range over which each of the hexatic phases is stable is small. We will report later the results of simulation studies of a three-layer PbGaGa system; the preliminary results from those calculations support the conclusion that while the influence of the layer of Ga adjacent to the Pb layer on its properties is very great, that of the second Ga layer on the properties of the Pb layer is very small.

II. BACKGROUND INFORMATION

A. Pseudopotential

The pseudopotential theory of the liquid-vapor interface of a metal has been described in Refs. [3–5], to which the reader is referred for details. We mention here only those details concerning the pseudopotential required for comprehension of the character of the calculations carried out. The pseudopotential Hamiltonian has the form

$$H = \sum_{i=1}^{N} \frac{\mathbf{p}_i^2}{2m_i} + \sum_{i=1}^{N} \sum_{j>i}^{N} \Phi_{eff}[|\mathbf{R}_i - \mathbf{R}_j|; n_e(\mathbf{r})] + U_0[\rho_0(\mathbf{r}), n_e(\mathbf{r})], \tag{1}$$

where $\mathbf{p}_i$ is the momentum of the ith atom with mass m_i, $\Phi_{eff}[|\mathbf{R}_i - \mathbf{R}_j|; n_e(\mathbf{r})]$ is the effective pair potential between atom i and atom j, $|\mathbf{R}_i - \mathbf{R}_j|$ is the distance between atom i and atom j, and $\rho_0(\mathbf{r})$ and $n_e(\mathbf{r})$ are reference jellium and electron densities. The functional $U_0[\rho_0(\mathbf{r}), n_e(\mathbf{r})]$ is a structure-independent contribution to the energy that is, however, dependent on the electron and jellium densities. The specific form of this functional that we have used is described in the paper by Zhao and Rice [3]; that paper reports the results of self-consistent Monte Carlo simulations of the density distribution along the normal in the interface of a dilute Pb in Ga alloy [3].

For the calculations reported in this paper, following the work of Zhao and Rice [3], we employed the nonlocal energy-independent model electron-ion pseudopotential proposed by Woo, Wang, and Matsuura [6,7]. It has the form

$$\hat{V}_{PS}^{ion}(r) = \sum_{l} \{\bar{V}_l(r) + [V_{1l}(r) - \bar{V}_l(r)]|R_{1l}\rangle\langle R_{1l}|\}|l\rangle\langle l|, \tag{2}$$

where $\bar{V}_l(r)$ is a pseudopotential average over all states other than the first valence state for a given angular momentum quantum number l, $|R_{1l}\rangle$ is the radial part of the wave function for the state, and $|l\rangle\langle l|$ is a projection onto the state with angular momentum quantum number l. With these definitions the model pseudopotential takes the form

$$V_{1l}(r) = \begin{cases} -B_{1l} + \dfrac{Z_l}{r}, & r < R_l, \\ -\dfrac{Z}{r}, & r \geqslant R_l, \end{cases} \tag{3}$$

where B_l, Z_l, and R_l are parameters that are usually determined by a pseudoeigenfunction expansion and perturbation

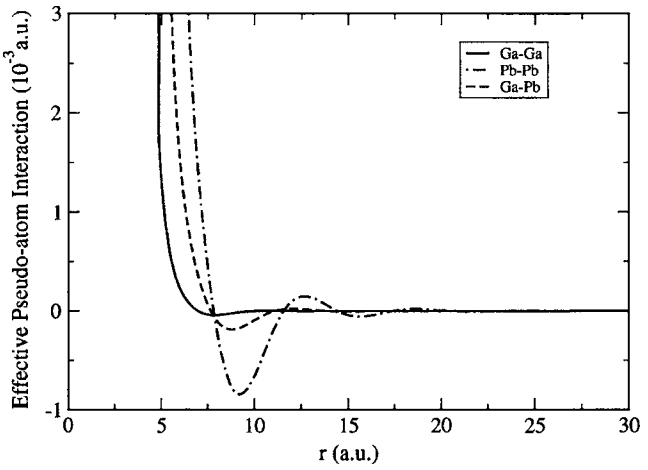

FIG. 1. The effective interion potentials for a Ga:Pb alloy.

theory. Z is the valence of the ion. The averaged pseudopotential $\bar{V}_l$ is calculated in the same fashion as is V_{1l} except for replacing the parameter B_{1l} with $\bar{B}_l$. Further details concerning the calculation of the electron-ion pseudopotential can be found in the report by Zhao and Rice [3].

The ion-ion pair potential used in the calculations reported below was calculated for a homogeneous metal with the density of the quasi-two-dimensional layer. In a homogeneous liquid metal with valence electron density the ion-ion pair interaction is [3,8,9]

$$\Phi(R_{ij}) = \frac{z_i^* z_j^*}{R_{ij}}\left\{1 - \frac{1}{\pi}\int_0^\infty [F_{ij}(q) + F_{ji}(q)]\frac{\sin(qR)}{q}dq\right\} + \Phi_{BM}(R_{ij}) + \Phi_{vW}(R_{ij}). \quad (4)$$

The first term in Eq. (4) is due to the direct Coulomb repulsion between ions with effective valence charges z_i^* and z_j^*, with $z_i^* z_j^* = Z_i Z_j - \bar{Z}_i \bar{Z}_j$ where Z is the true valence charge and $\bar{Z}$ is the depletion hole charge that originates from the orthogonality condition between the valence and core electron wave functions. The second term is an indirect interaction mediated by the conduction electrons, the so-called band structure energy. This contribution to the energy tends to offset the effect of the strong Coulomb repulsion and thus lowers the energy of the system. $\Phi_{BM}(R_{ij})$ is the Born-Mayer core-core repulsion interaction [10], and $\Phi_{vW}(R_{ij})$ is the van der Waals polarization interaction between the ion cores [9]. In general, the latter two contributions to the energy are much smaller than the other contributions to the energy of the liquid metal. Finally, $F(q)$ is the normalized energy-wave number characteristic function. We have used the form of this function derived by Shaw [8] (also see the paper by Zhao *et al.* [5]). The calculated effective interionic potentials are shown in Fig. 1.

B. Computational details

A simulation sample with an adequate number of atoms per stratum to support long-ranged in-plane crystalline order and with sufficient depth to accurately represent the bulk liquid is too large for the computational resources available to us. We have compromised by using the available experimental information to design a simulation sample that will permit an accurate representation of what we believe to be the most important characteristics of the liquid-vapor interface of a dilute PbGa alloy. Specifically, we have accepted that the density distribution along the normal is stratified and that the outermost stratum is a monolayer of Pb. Consequently, we have constructed our simulation samples to have a large number of atoms per layer and just enough layers to adequately represent the influence of the Ga on the Pb layer. Taking advantage of the stratification of the liquid-vapor interface we have restricted the Pb and Ga atoms to their respective layers. We have studied four model systems: a Q2D monolayer of Pb atoms, a strictly 2D monolayer of Pb atoms (using the original COR potential [4] and the nonlocal pseudopotential described in the last section), and a two-layer system consisting of a monolayer of Pb atoms atop a monolayer of Ga atoms. Systems of different size were examined, some with about 5000 atoms. The unadorned Q2D Pb monolayer model was studied to provide a connection between the current studies and those reported by Chekmarev, Oxtoby, and Rice [4]; the strictly 2D models were studied to determine the limiting behavior of the Pb monolayer in the absence of out-of-plane motion, specifically the influence of out-of-plane motion on the range of stability of the hexatic phase.

For the simulations of the Q2D Pb monolayer, 2016 Pb atoms were placed in a rectangular box in the xy plane; the ratio of the lengths of the sides of the box was $7/4\sqrt{3}$. We chose this geometry to accommodate a perfect two-dimensional hexagonal crystal, while keeping the box shape nearly square. The box area is fixed at the value for which the 2D density of the atoms equals the observed density of Pb atoms—namely, 9.87 nm^{-2}. The Pb atoms are permitted to move perpendicular to the xy plane, with the motion in the z direction constrained by an external harmonic potential. The strength of the harmonic potential was chosen so that the average layer thickness is the same (within the experimental uncertainty) as that observed. Periodic boundary conditions were applied in both the x and y directions, but not in the z direction.

The 2D simulations were carried out for a sample containing 10 044 Pb atoms. The initial configuration was taken to be a perfect hexagonal lattice in a box with side lengths in the ratio $93/54\sqrt{3}$. Our simulations of the two-layer GaPb system had 2016 Pb atoms in one layer and 2804 Ga atoms in the other layer, for a total of 4820 atoms. The number of Ga atoms in the simulation box was chosen to reproduce the density of the Ga layer immediately below the Pb monolayer in the stratified liquid-vapor interface of the alloy. That density is 13.7 nm^{-2}; it was determined from the observed ratio of densities of the Pb monolayer and the adjacent Ga layer. To accommodate a perfect 2D crystal, the simulation box in the xy plane had sides with lengths in the ratio $7/4\sqrt{3}$. The Pb atoms and the Ga atoms were constrained to remain in their respective layers by two different harmonic potentials in the z direction. The distance between the centers of these two harmonic potentials was set equal to the sum of the effective atomic radii of the Pb and Ga atoms.

We have carried out both *NVT* and *NpT* simulations, the former motivated by the suggestion, from the experimental data, that there is only a very small or possibly zero-density change in the quasi-2D phase transition. The latter simulations were undertaken to examine the accuracy of this suggestion. The results of the *NpT* simulations do show that the density change across the transition is very small, possibly zero in an infinite sample, and the fluctuations in the immediate vicinity of the transition temperature are reduced from those observed in the *NVT* simulations, thereby permitting a more accurate determination of the temperature dependence of the order parameters.

The starting configuration for our *NVT* ensemble simulations of the isolated Pb layer was perfect 2D hexagonal packing. For the two-layer system the starting configuration of the Pb atoms also was perfect 2D hexagonal packing. However, because our simulation box is not designed to hold a perfect 2D Ga crystal, the starting configuration for the Ga atoms was random 2D packing subject to the constraint of no atom-atom overlap. In both systems, the initial positions of the atoms in the z direction were at the minima of the respective constraining harmonic potentials (the mean positions of the layers). Since the experimental data suggest that there is zero or a very small change in the density of the Pb monolayer across the transition, all two-dimensional particle densities were fixed throughout the *NVT* simulations.

In the *NpT* ensemble simulations of the Pb monolayer the surface pressure was fixed at 2.100 N/m for the 2D system and 1.464 N/m for the Q2D system; for the PbGa bilayer, it was fixed at 2.786 N/m. These values of the surface pressure were chosen to keep the surface density close to the value fixed in the *NVT* ensemble simulations when the temperature is close to the transition point of the Pb monolayer. The area of the simulation box was allowed to fluctuate by altering one or the other of its side lengths randomly.

In all of our simulations at least several millions of Monte Carlo steps were taken to equilibrate the system, and physical properties were calculated every 2048 Monte Carlo steps thereafter. In our notation, one Monte Carlo step involves the displacement of every particle in the system once. The achievement of equilibrium was monitored by the average values of physical parameters, such as the energy. The simulations were continued until these average values were constant within their fluctuation ranges. In the two-layer simulations the convergence is slow near the transition temperature. In that case we used at least 1×10^7 Monte Carlo steps to reach the equilibrium state, and physical properties were calculated every 2048 Monte Carlo steps thereafter for 4×10^6 steps.

To monitor the structural change occurring in the melting process, we elected to work with two sets of order parameters, which are defined in a similar way as in the paper by Chekmarev *et al.* [4]. One set consists of the global bond-orientation and global translational order parameters, denoted GOOP and GTOP, respectively. These quantities provide information on the overall character of the melting process.

Adhering to the widely used convention, for each particle we define

$$\psi_{6i}=\frac{1}{n_i}\sum_{j}^{n_i}\exp[i6\theta(R_{ij})], \tag{5}$$

in which n_i is the number of nearest neighbors (NN) of the ith particle and θ_{ij} designates the angle between the imaginary bond R_{ij} connecting particles i and j and an arbitrary axis x. The NN list was compiled for each atom in a chosen configuration from the associated Voronoi polygon mapping of that configuration [11].

For a perfect 2D hexagonal solid, $|\psi_{6i}|^2=1$. In contrast, for a disordered system the peak of the distribution of $|\psi_{6i}|^2$ is shifted toward smaller values (ultimately zero), thereby signaling the loss of the bond orientation symmetry in the first neighbor shell of an atom.

The GOOP is defined by [12,13]

$$\Psi_6=\frac{1}{N}\left|\sum_{i=1}^{N}\psi_{6i}\right|, \tag{6}$$

where the summation extends over all N atoms in the box. Similarly, the global translational order parameter is defined by [12]

$$\Psi_T=\frac{1}{N}\left|\sum_{i=1}^{N}\exp(i\mathbf{G}\cdot\mathbf{R}_i)\right|. \tag{7}$$

In Eq. (7), $\mathbf{G}$ denotes a reciprocal lattice vector of the triangular lattice and $\mathbf{R}_i$ is the position vector of the ith particle. A crude identification of the thermodynamically stable phases that participate in the process of melting of a quasi-2D metallic system can be deduced from the magnitudes of the calculated values of the GOOP and GTOP. For a disordered liquid phase these values must be much less than unity. In contrast, in a typical 2D solid one finds that $0<\Psi_6$ and $\Psi_T<1$, with these values rapidly approaching unity as the structure becomes progressively more ordered and more nearly defect free. More insight can be gained from an analysis of the correlation lengths associated with the GOOP and GTOP. This information can be extracted from the decays of the envelopes of the corresponding correlation functions—namely, the bond orientation correlation function

$$g_6(R)=\langle\psi_6^*(0)\psi_6(\mathbf{R})\rangle \tag{8}$$

and the pair correlation function

$$g(\mathbf{R})=\frac{2V}{N(N-1)}\left\langle\sum_{i=1}^{N}\sum_{j>i}^{N}\delta(\mathbf{R}-\mathbf{R}_{ij})\right\rangle, \tag{9}$$

where $\langle\cdots\rangle$ refers to an ensemble average. In the above expressions, the vectors and distances in the arguments are the projections of the 3D quantities onto the xy plane.

Additional information concerning the nature of a phase can be obtained from an analysis of the diffraction pattern associated with the particle configuration in that phase. We have computed both the 2D static structure factor $S(\mathbf{q}_{xy})$ and the angle-averaged static structure factor $S(q_{xy})$. The structure factor is defined by

$$S(\mathbf{q}_{xy}) = \frac{1}{N}\left\langle \sum_{i=1}^{N}\sum_{j=1}^{N} \exp[i\mathbf{q}_{xy}\cdot(\mathbf{R}_i - \mathbf{R}_j)] \right\rangle, \quad (10)$$

where $\mathbf{q}_{xy}$ is a 2D wave vector and $\mathbf{R}_i$ and $\mathbf{R}_j$ are 2D projections of the position vectors of particles i and j onto the xy plane. When averaged over angles, the above expression reduces to

$$S(q_{xy}) = 1 + \frac{2}{N}\left\langle \sum_{R_{ij}} J_0(q_{xy}R_{ij}) \right\rangle. \quad (11)$$

In Eq. (11), J_0 designates the zeroth-order regular Bessel function and the sum runs over all distinct pairs of particles. Due to the small size of the simulation sample, we cannot use Eq. (10) to capture the correct long-wavelength behavior of the structure factor. Numerically, this would inevitably result in spurious fluctuations of $S(q_{xy})$ in the small q_{xy} domain. Still, for the simulation samples we have studied, we found that the positions and magnitudes of the first several peaks in $S(q_{xy})$ can be established with confidence.

A final word concerning the computational cost of our procedure is in order. Because our pseudopotential is relatively long ranged, the number of neighboring atoms that interact with each atom is large, which makes the calculation of the potential energy very expensive. In our simulations, the average numbers of atoms that interact with a given atom are 80 and 180 for the one-layer and two-layer models, respectively. The two-layer simulation sample had 4820 atoms. For this model the computational speed is 2.2 Monte Carlo steps per second using a 1.6-GHz AMD Athlon MP processor. Close to the transition temperature runs of at least several million Monte Carlo steps are needed to equilibrate the system.

III. RESULTS

A. Pb monolayer

We discuss in this section the results obtained from simulations of the Q2D Pb monolayer and from simulations of the strictly 2D Pb monolayer. We use these results to examine the effect of small-amplitude out-of-plane motion on the stability of the monolayer and the character of the melting transition. In this section we focus attention on the results obtained with the *NpT* ensemble; we briefly report and discuss the results obtained using the *NVT* ensemble in the Appendix.

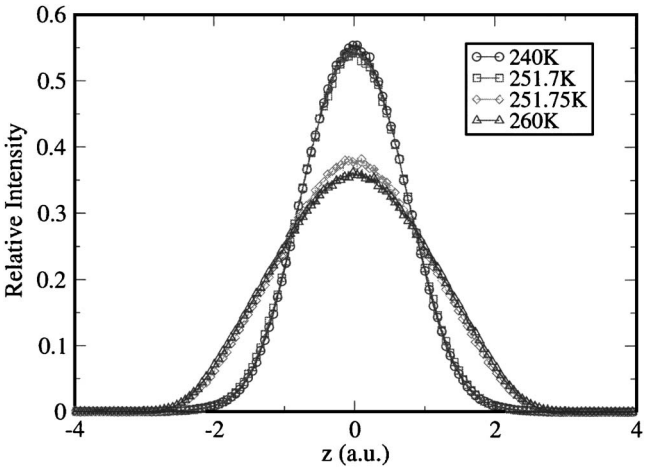

FIG. 3. The out-of-plane distribution of a Q2D Pb layer around the melting point.

The average potential energy per particle in the Q2D Pb monolayer obtained from the *NpT* ensemble simulations is shown in Fig. 2. There is a discontinuous jump in the potential energy per atom at about 251 K that we associate with the transition from the two-dimensional crystal to a less-ordered phase. We will show below that the most likely value for the transition temperature is between 251.70 and 251.75 K. The potential energy change across the transition corresponds to an entropy change of $0.44k_B$. We display in Fig. 3 the distribution of out-of-plane atomic amplitude for several temperatures around the transition temperature. Figure 4 displays the standard deviation of the z distribution of the monolayer. These z-amplitude distribution functions also exhibit a discontinuous change in peak value between 251.70 and 251.75 K. The change in magnitude of the out-of-plane motion amounts to about 40% of the peak value. The change

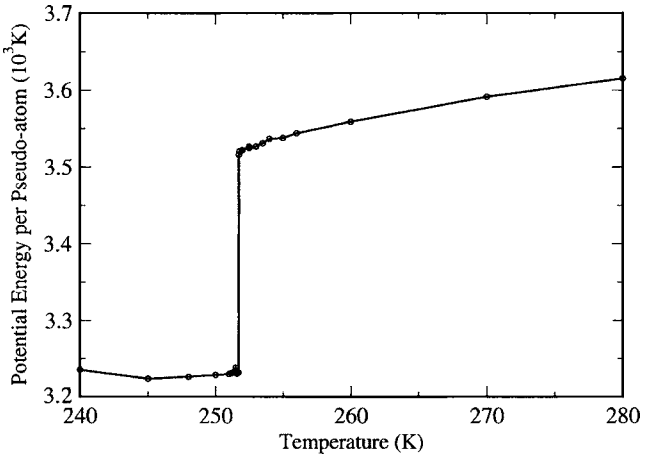

FIG. 2. The average potential energy per atom of a Q2D Pb layer around the melting point.

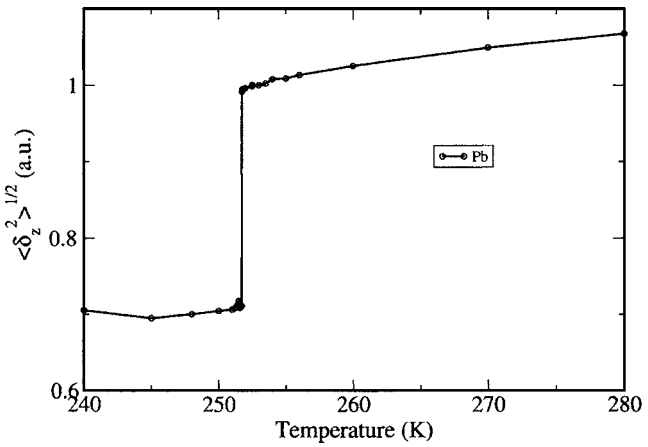

FIG. 4. The standard deviation of the out-of-plane distribution of a Q2D Pb layer around the melting point.

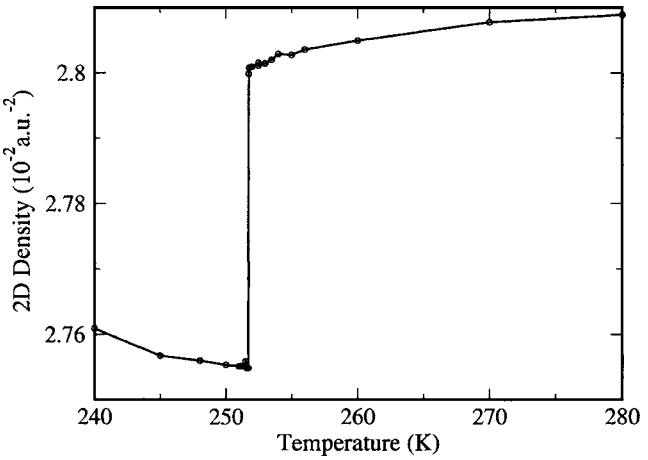

FIG. 5. The two-dimensional density of a Q2D Pb layer around the melting point.

in the two-dimensional density of the monolayer as the transition is traversed is shown in Fig. 5. The two-dimensional density changes discontinuously, indicative of a first-order transition. However, the increase in two-dimensional density in the disordered phase is accompanied by a large increase in amplitude of the out-of-plane motion of the Pb atoms, with the consequence that the three-dimensional density of the Pb layer is changed very little across the transition.

Figure 6 displays the global translational and bond orientation order parameters for several temperatures close to the transition temperature, which is between 251.70 and 251.75 K. Just above the transition temperature the Pb monolayer appears to have only very slightly greater bond orientation order than translational order. We infer that the isolated monolayer of Pb does not support a hexatic phase intermediate between the crystal and liquid phases. Our conclusion concerning the existence of a Q2D crystal-to-hexatic transition in the Pb monolayer differs from that of Chekmarev, Oxtoby, and Rice [4]. We will discuss the origin of this difference later in this paper.

Figure 7 displays the pair correlation for several temperatures close to the transition temperature, and Fig. 8 displays

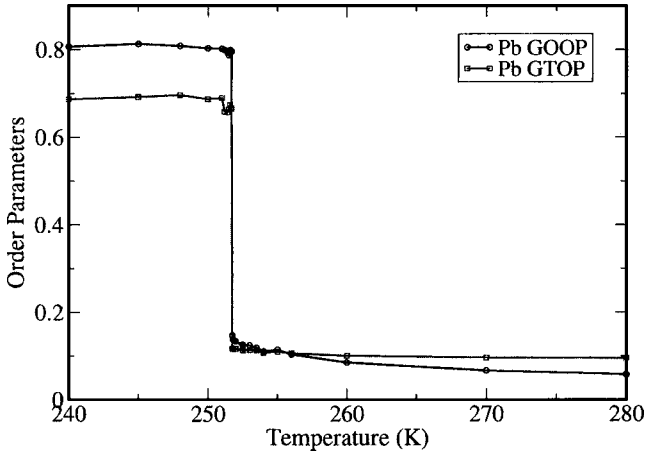

FIG. 6. The order parameters of a Q2D Pb layer around the melting point. Lines are shown to guide the eye. The translational order parameters are shown in red.

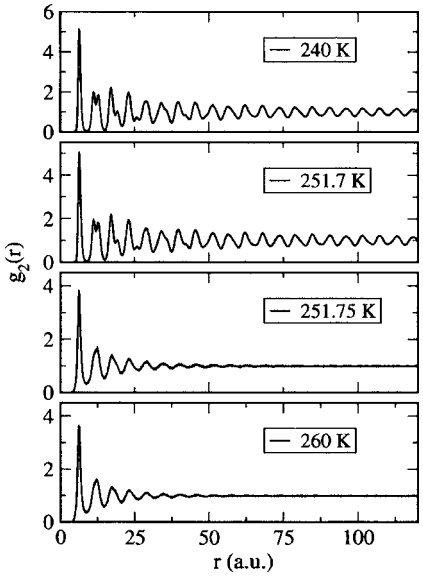

FIG. 7. The pair correlation functions of a Q2D Pb layer around the melting point.

the bond orientation correlation function for the same temperatures. These correlation functions clearly show that at 250 K the Q2D Pb monolayer is crystalline and at 260 K it is liquid.

It is our opinion that, given the limited size of simulation samples, the best signature of hexatic ordering is the shape of the diffraction peak in the calculated structure factor of the Q2D system. Figures 9 and 10 display, respectively, calculations of $S(q_{xy})$ as a function of q_{xy} at several temperatures and the powder diffraction pattern $S(q)$. We calculated $S(q)$ by Fourier inversion of the real-space pair correlation function $g_2(R)$. Just above the phase transition temperature the amplitude of the first diffraction peak is about 5, a value rather close to that expected from the accurate empirical rule

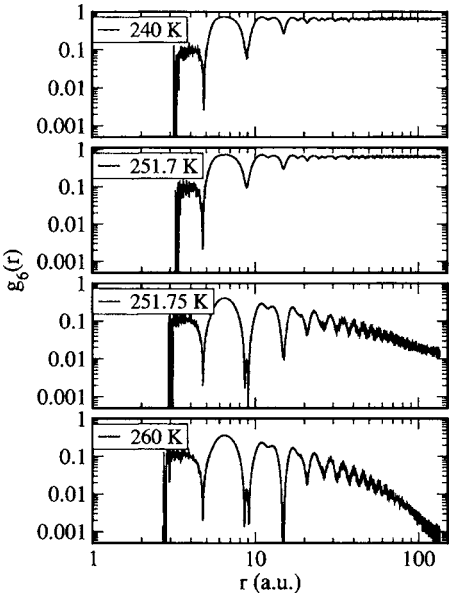

FIG. 8. The orientation correlation functions of a Q2D Pb layer around the melting point.

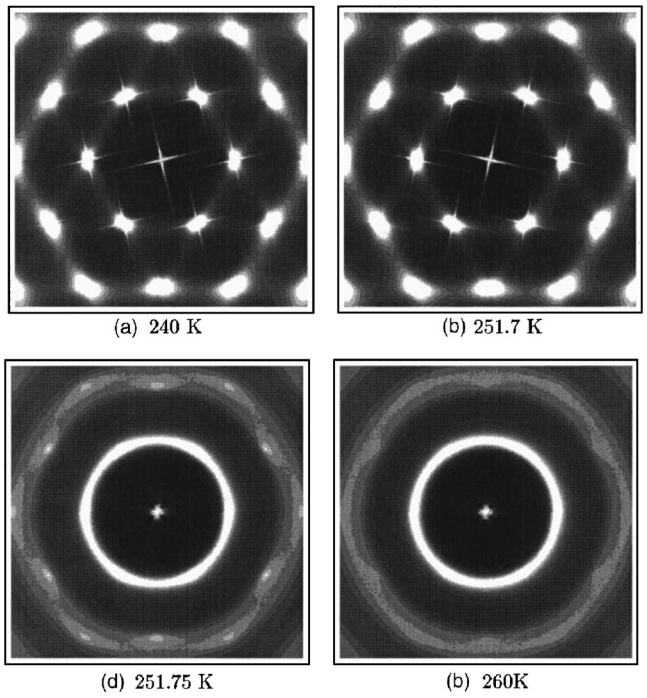

FIG. 9. The two-dimensional scattering pattern $S(q_{xy})$ of a Q2D Pb layer. Higher intensity is shown by the lighter gray level.

that the liquid-to-solid phase transition occurs when the amplitude of the first peak of the liquid structure function is 5 [14,15]. Some azimuthal intensity patterns are shown in Fig. 11. We were unable to obtain a satisfactory fit of the angular (azimuthal) variation of the intensity of the principal scattering peak obtained from the calculated $S(q)$ to a square-root Lorentzian (SRL) function [16], the functional form that is a diagnostic for diffraction from a hexatic phase. This observation is a critical component of our inference that the isolated monolayer of Pb does not support a hexatic phase intermediate between the crystal and liquid phases.

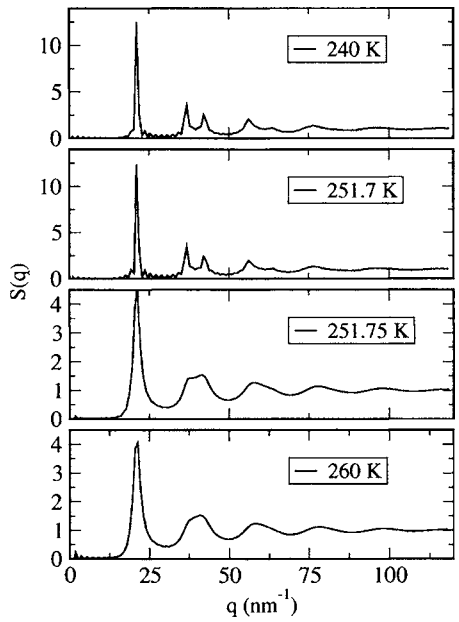

FIG. 10. The powder scattering pattern $S(q)$ of a Q2D Pb layer.

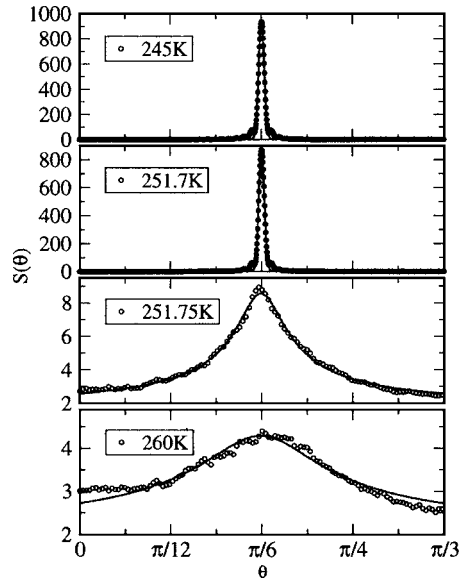

FIG. 11. The azimuthal variation of the intensity of the principal scattering peak of a Q2D Pb layer. Solid lines show model fitting. A Gaussian model is used for the crystalline phase, and a square-root Lorentzian (SRL) model is used for temperatures above the melting point.

As indicated earlier, we also carried out simulations of the Q2D Pb monolayer in the *NVT* ensemble. The results obtained are nearly identical with those obtained from simulations in the *NpT* ensemble, except that fluctuations in the former are larger than in the latter and the approach to equilibrium in the former is slower than in the latter. We show in Fig. 12, for comparison with the data displayed in Fig. 6, the global translational and bond orientation order parameters for several temperatures close to the transition temperature. The major difference between these data sets is in the value of the global bond orientation order parameter immediately above the transition temperature; this value is larger in the *NVT* simulations than in the *NpT* simulations, a difference that we attribute to fluctuations in the finite sample.

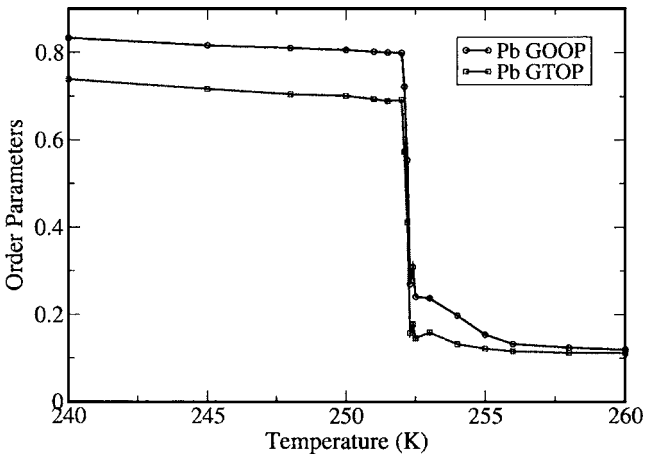

FIG. 12. The order parameters of a Q2D Pb layer, calculated in the *NVT* ensemble. The simulation box contains 2016 atoms.

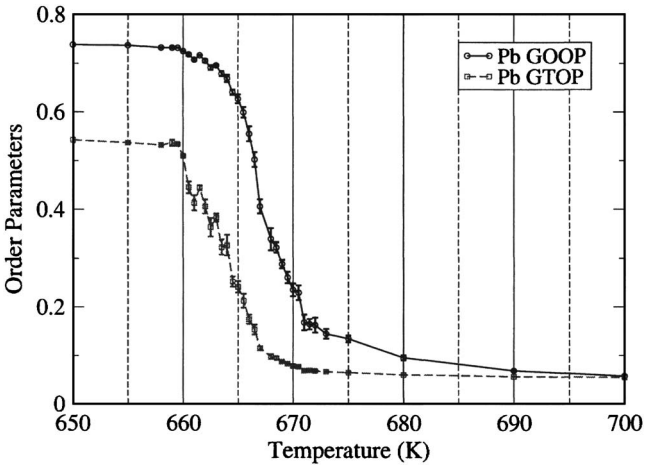

FIG. 13. The order parameters of a 2D Pb layer, calculated in the *NpT* ensemble with the EIMP pseudopotential [5–7]. The simulation box contains 10 044 atoms. Lines are shown to guide the eye.

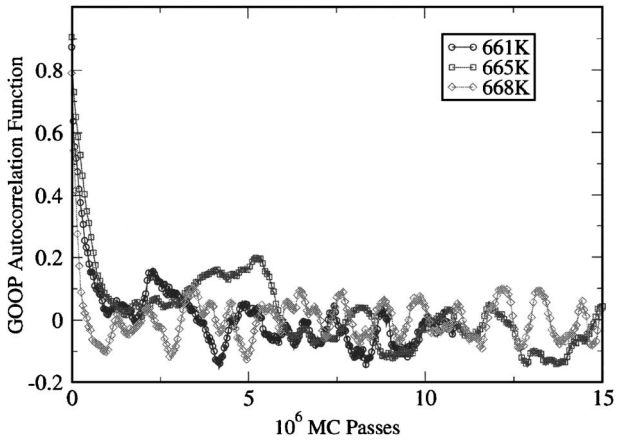

FIG. 14. The autocorrelation functions of the global orientational order parameter of a strictly 2D Pb layer. The average order parameters are shown in Fig. 13. These three temperatures are chosen to be slightly higher than the transition temperatures shown in Fig. 13.

We have also carried out extensive simulations of a strictly 2D Pb monolayer, using two pseudopotentials. Specifically, we have carried out calculations both with the nonlocal pseudopotential used by Zhao and Rice [3] and the local pseudopotential used by Chekmarev, Oxtoby, and Rice [4]. In both cases the lack of out-of-plane motion greatly increases the transition temperature. We had difficulties in equilibrating the 2D system around the transition point when using the local pseudopotential used by Chekmarev, Oxtoby, and Rice [4]. Figure 13 displays the order parameters of a strictly 2D Pb monolayer, using the nonlocal pseudopotential. With this nonlocal pseudopotential, the transition between the ordered solid and the disordered high-temperature phases appears to be a three-stage process. For temperatures up 660 K, both translational and orientational order parameters imply that there is an ordered solid structure. Between 660 and 660.5 K, there is a small but clearly discontinuous change of the translational order parameter, while no clear change of the orientational order parameter is found across this temperature range. A second first-order phase transition occurs between 664 and 664.5 K, similar to the first transition, but different in that the orientational order parameter also shows a weak discontinuous change accompanying the sudden decrease of the translational order parameter. A third transition occurs around 666.5 K, when the orientational order parameter decreases abruptly; the change in the translational order parameter is small in magnitude around this temperature. At higher temperatures, both order parameters continue to decrease and eventually imply the formation of an isotropic liquid. These data strongly support the view that incorporation of the small-amplitude out-of-plane motion that must be present in a real monolayer makes an important contribution to the thermodynamic properties of that monolayer.

We found the convergence of simulations to be significantly slower with the larger number of particles in the simulation box. Because the order parameter changes at transitions are smaller in magnitude than in the Q2D monolayer case (see Fig. 6) and in the bilayer case (see Fig. 15 below), autocorrelation functions of the order parameters along the Monte Carlo pseudotime evolution have been calculated to show the speed of convergence. Figure 14 displays the GOOP autocorrelation functions at several temperatures within the transition temperature range. The autocorrelation function of the GTOP is similar to that of the GOOP, due to positive correlation between these two order parameters. The central peak of the autocorrelation functions decays on a Monte Carlo pass scale of about 4×10^5 steps, which is at least 10 times smaller than the total simulation Monte Carlo pass numbers we run within the transition temperature range. The autocorrelation functions do show that there is slower decay at longer time, but no obvious time constant can be identified.

B. Ga-Pb bilayer

We now examine the properties of the quasi-two-dimensional monolayer of Pb when it is in contact with a Q2D monolayer of Ga. We use this two-layer model to assess the effect of the Ga substrate on the Pb monolayer segregated in the liquid-vapor interface of a dilute Pb in Ga alloy.

Our model captures correctly the experimental fact that Q2D crystalline Pb can be supported on liquid Ga. We display in Fig. 15 the global orientation order parameter and the translational order parameter for the PbGa two-layer system as a function of temperature and in Figs. 16 and 17 the pair correlation and bond orientation correlation functions for the Pb and Ga layers in that system. Clearly, there is a transition from a Q2D crystalline state to a disordered state in the Ga layer at about 380 K, at which temperature the Pb layer remains in a Q2D crystalline state. The Pb layer melts at 413 K. We note that just above 380 K the GOOP of the Ga layer is about 0.6 and the GTOP of the Ga layer is about 0.3. These values for the order parameters suggest that the phase that is formed has hexatic structure. The further destruction of order as the hexatic phase is heated from 381 to 400 K appears to be a continuous process. At 400 K both the GOOP and GTOP of the Ga layer have values that are typical for a liquid phase.

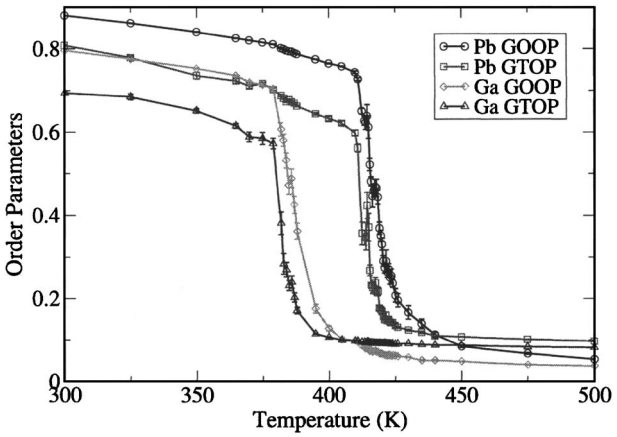

FIG. 15. The order parameters of a PbGa bilayer, calculated in the NpT ensemble with the EIMP pseudopotentials [5–7]. The simulation box contains 4820 atoms. Lines are shown to guide the eye.

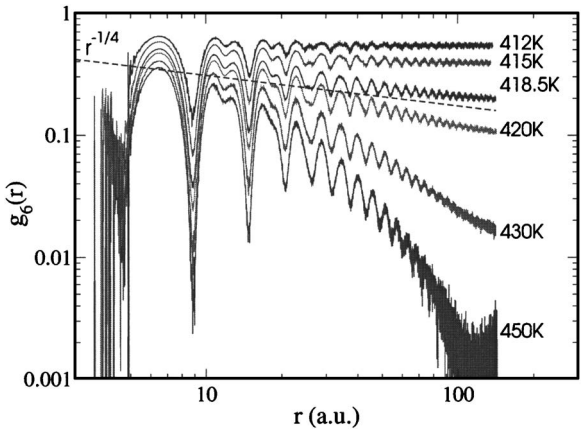

FIG. 17. The Pb bond orientation correlation functions of a PbGa bilayer. The dashed line shows the $r^{1/4}$ pattern, which is predicted by the KTHNY theory as the extreme value possible for a hexatic phase.

The GOOP and GTOP temperature dependences shown in Fig. 15 suggest that in the two-layer system the Q2D crystalline Pb layer undergoes three transitions en route to the Q2D liquid phase. The first stage in the melting, between 412.0 and 412.5 K, involves discontinuous decreases in both the GOOP and GTOP for the Pb layer. The higher-temperature phase that is formed is stable from 412.5 to 415.0 K, and it has a hexatic structure. At a temperature between 415.0 and 415.5 K there is another discontinuous change in the GOOP and a small discontinuous change in the GTOP. The higher-temperature phase that is formed by this transition also has hexatic structure. The temperature range over which this second hexatic phase is stable is approximately 3 K, from about 415.5 to 418.5 K. Between 418.5 and 419.0 K there are weak discontinuous jumps in both the GOOP and GTOP, and a more disordered phase is formed. For temperatures above 423 K the Pb monolayer is a Q2D liquid.

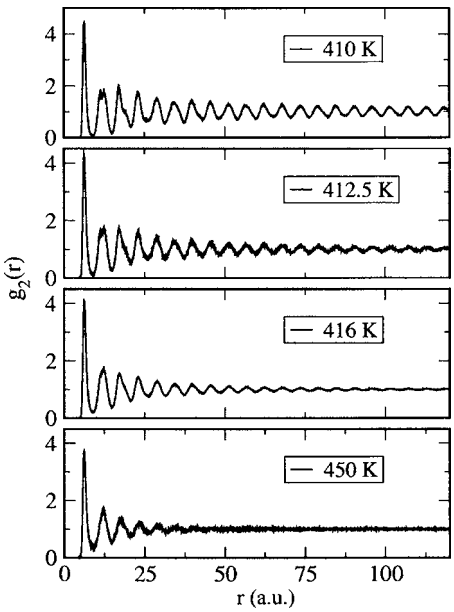

FIG. 16. The Pb pair correlation functions of a PbGa bilayer. Patterns are shown, respectively, for the crystalline, hexatic (I), hexatic (II), and liquid phases.

These inferences are supported by the results displayed in Figs. 16 and 17. When the temperature is between 412.5 and 418.0 K the envelope of the bond orientation correlation function of the Pb layer, $g_6(r)$, decays algebraically. At 418.5 K, which is just below the third transition temperature of the Pb layer, the algebraic decay is very close to $r^{1/4}$ which, according to the Kosterlitz-Thouless-Halperin-Nelson-Young (KTHNY) theory [17–21], is the extreme value possible for a hexatic phase. The decay of the bond orientation correlation function is also close to algebraic in form after the third transition of the Pb layer, between 418.5 and 419.0 K. The decay is close to exponential in form for temperatures higher than 450 K. The transition from algebraic decay to exponential decay of the envelope of $g_6(r)$ is smooth. We infer that the Pb layer of the bilayer is liquid when the temperature exceeds 419 K even though the value of the GOOP might be interpreted as characteristic of a hexatic phase. To corroborate this inference we display, in Fig. 18, $S(q_{xy})$ for the Pb layer of the bilayer. Between 412.5 and 418.5 K, the structure function exhibits stretching of the diffraction intensity in the azimuthal direction. The stretching of the diffraction spot in the azimuthal direction is greater in the second hexatic phase, formed at higher temperature, than in the lower-temperature hexatic phase. There is further azimuthal stretching of the intensity just above 418.5–419.0 K, and this residue of bond orientation order is consistent with the relatively high GOOP within this temperature range. Noting that $S(q_{xy})$ appears to be the superposition of weak diffraction peaks and a diffraction ring we interpret the form of $S(q_{xy})$ to arise from heterophase fluctuations in the finite system we simulate. Figure 19 displays the powder diffraction pattern of the Pb layer of the bilayer, $S(q)$, calculated from the pair correlation function. The bond orientation order and the translational order in the hexatic phase are greater than in the liquid phase, and this is clearly seen when the $S(q)$ for 414 and 418 K are compared to that

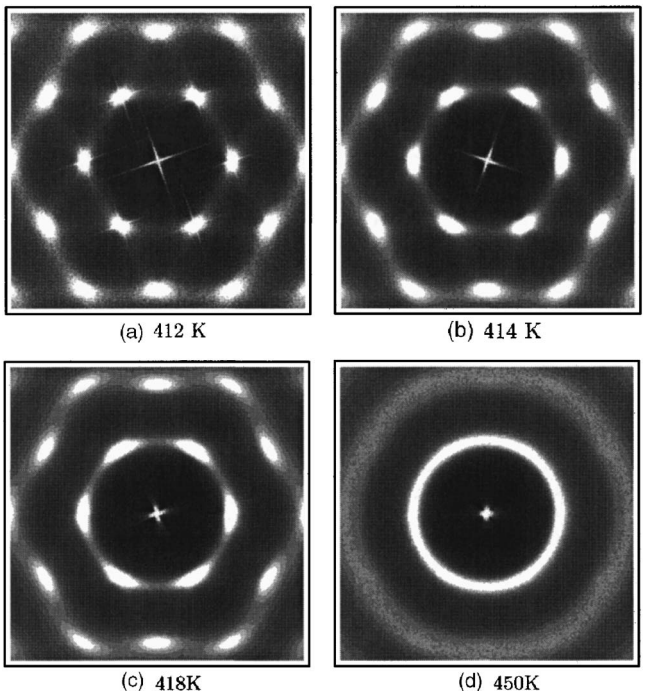

FIG. 18. The two-dimensional scattering pattern $S(q_{xy})$ for the Pb layer in a PbGa bilayer.

for 450 K. Figure 20 displays the azimuthal variation of the intensity of the principal scattering peak obtained from the calculated $S(q)$. The differentiation between a liquid phase and a hexatic phase is based on the square-root Lorentzian fit to the shape of the diffraction peak for the latter [16]. The diffraction peak at 410 K, at which temperature the Q2D crystalline phase is stable, is well fitted with a Gaussian function. The diffraction peaks at 414 and 417 K, at which temperatures we argue there are two different hexatic phases,

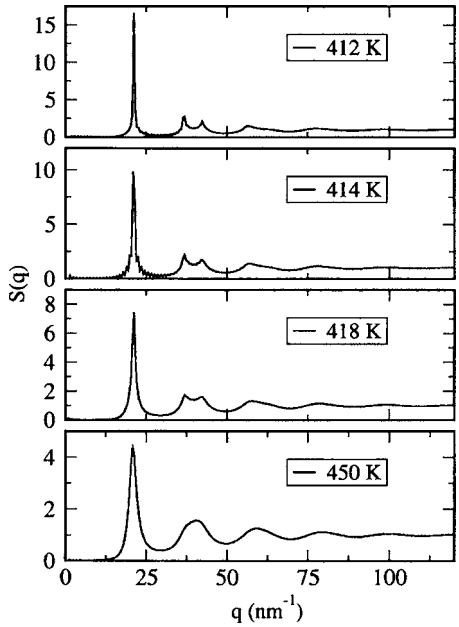

FIG. 19. The powder scattering pattern $S(q)$ for the Pb layer in a PbGa bilayer.

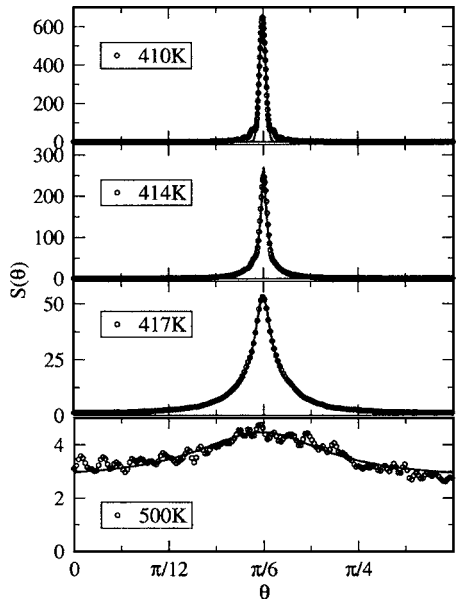

FIG. 20. The azimuthal variation of the intensity of the principal scattering peak for the Pb layer in a PbGa bilayer.

are well fitted with square-root Lorentzian functions. The difference between the two hexatic phases is manifested in the widths of the azimuthal distributions of intensity of the respective $S(q_{xy})$; that of the higher-temperature hexatic is about 3 times greater than that of the lower-temperature hexatic. As already noted, we interpret the very weak diffraction peak at 500 K, at which temperature the liquid phase is stable, to be the consequence of heterophase fluctuations in our finite system; the line shape is well fitted to a square-root Lorentzian function.

We display in Fig. 21 the analog of Fig. 2—namely, the average total potential energy as a function of temperature. In Fig. 22 we show the average potential per particle as a function of temperature for Pb and Ga atoms. When one layer melts, the average potential of that layer increases, while the average potential of the other layer decreases. There is a much smaller change in the potential energy per

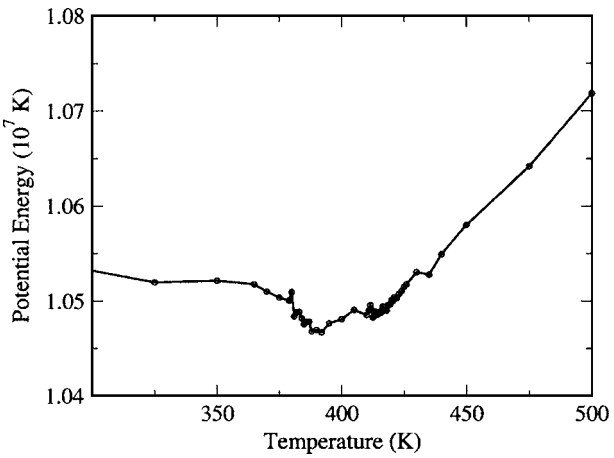

FIG. 21. The total potential energy of a PbGa bilayer around the Pb melting point.

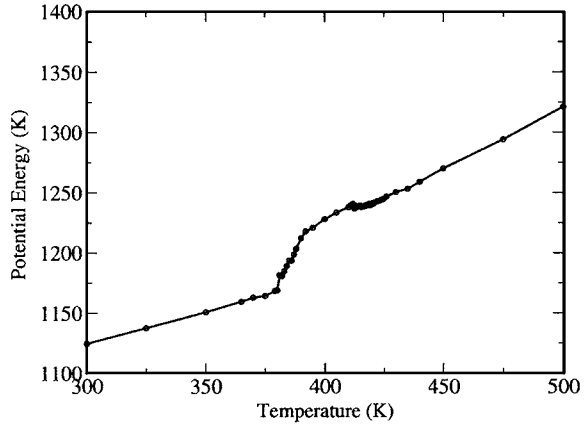

(a) The potential energy of the Ga layer in a PbGa bilayer.

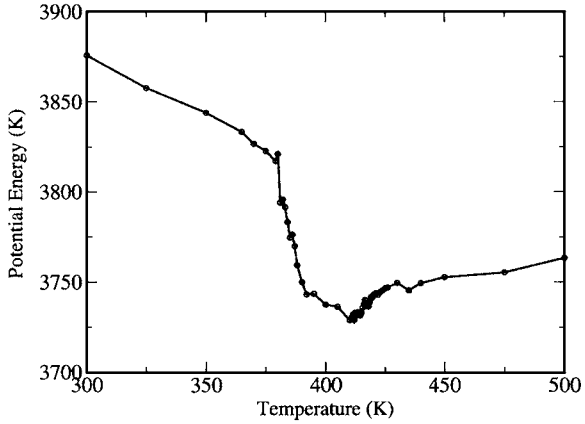

(b) The potential energy of the Pb layer in a PbGa bilayer.

FIG. 22. The potential energy of each layer in a PbGa bilayer. The potential energy per particle is shown.

atom at the Pb layer transition temperature in the bilayer than in the monolayer. Figure 23 displays the analog of Fig. 5—namely, the two-dimensional density as a function of temperature. The two-dimensional density decreases with increasing temperature throughout our simulation temperature range. There is a small discontinuous density decrease at each of the first order transitions that occur in the bilayer system (one in the Ga layer and two in the Pb layer). We

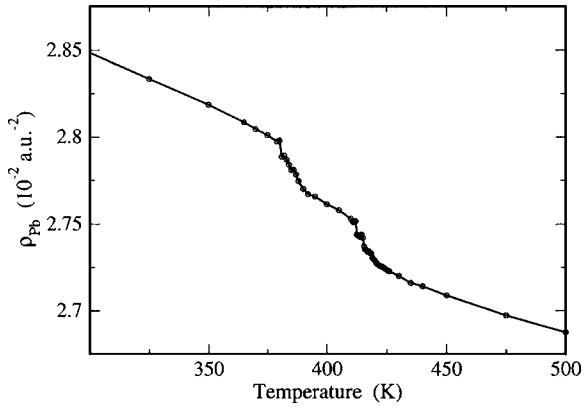

FIG. 23. The two-dimensional density of the Pb layer in a PbGa bilayer around the Pb melting point.

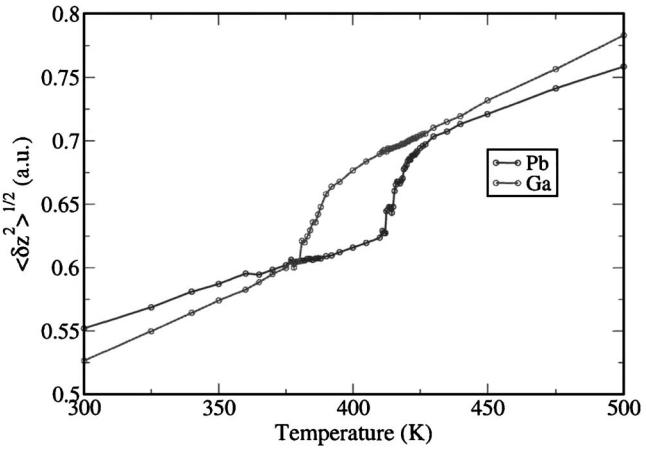

FIG. 24. The temperature dependences of the out-of-plane amplitudes $\langle \delta_z^2 \rangle^{1/2}$ of the Pb and Ga atoms in the bilayer.

display in Fig. 24 the temperature dependences of the out-of-plane amplitudes $\langle \delta_z^2 \rangle^{1/2}$ of the Pb and Ga atoms in the bilayer. The distributions of atomic amplitudes are close to Gaussian at all temperatures, but there is a noticeable deviation from the Gaussian shape for displacements in the region between the two layers. The amplitude of out-of-plane motion in each layer increases at the melting temperature of that layer and seems to be insensitive to the transition that takes place in the other layer. At temperatures other than the transition temperatures the standard deviation of the out-of-plane amplitude distribution increases linearly with temperature. There are small discontinuous changes in $\langle \delta_z^2 \rangle$ when the corresponding layer undergoes a first-order transition. The change in amplitude of the out-of-plane motion when the Q2D crystalline layer is completely transformed to a Q2D liquid is 10% after correction for the linear dependence of $\langle \delta_z^2 \rangle$ on T. This change in $\langle \delta_z^2 \rangle$ at the transition is much smaller than the 40% change found in the Q2D Pb monolayer simulations.

IV. DISCUSSION

A segregated monolayer of Pb supported on liquid Ga, such as occurs in the liquid-vapor interface of a dilute Pb in Ga alloy, is a complex many-body system. We have examined two simple models of this interface—namely, that it can be treated as a Q2D monolayer or as a Q2D bilayer consisting of weakly interacting Pb and Ga layers. The interactions in the system have been determined using the pseudopotential representation of Zhao and Rice [3]. Although our model is a drastic simplification of reality, we expect that when a reasonable pseudopotential is used the qualitative features of the in-plane structure of the liquid-vapor interface of this alloy will be properly described.

The interpretation of the simulation data proffered in the preceding section made extensive use of the conceptual structure developed for the theory of melting of a two-dimensional ordered solid. The validity of that interpretation depends on establishing the accuracy with which the liquid-vapor interface of a metal can be represented as a two-

dimensional system. It is immediately obvious that the liquid-vapor interface of a metal is, at best, a quasi-two-dimensional system. This categorization is intended to emphasize that the properties of the outermost layer of that interface are affected both by out-of-plane motion of the atoms of that layer and by contact with the substrate liquid. Our simulations show that the interaction between an ordered Pb monolayer and a liquid Ga monolayer lowers the melting point of the former and changes the character of the phase transition. The isolated Q2D monolayer of Pb does not support a hexatic phase intermediate between the crystal and liquid phases, whereas the Q2D PbGa bilayer does. Our simulations also show that the melting point of the Q2D Pb monolayer is sensitive to the amplitude of out-of-plane motion.

Other work from this laboratory has established that a liquid monolayer of a solute segregated in the liquid vapor interface of an alloy, as occurs for dilute alloys of Sn in Ga or Bi in Ga, has an effective surface tension very different from (much greater than) the value obtained by extrapolation of the pure solute liquid surface tension to the temperature of observation. The difference between the measured and extrapolated surface tensions is another signature of the importance of the interaction between the segregated monolayer and the substrate. This conclusion follows from the form of the Triezenberg-Zwanzig representation of the surface tension of the liquid-vapor interface [22],

$$\gamma = \frac{k_B T}{4} \sum_{\alpha\beta} \int dz_\alpha \int dz_\beta \int dR_{\alpha\beta} \frac{d\rho(z_\alpha)}{dz_\alpha} \frac{d\rho(z_\beta)}{dz_\beta} \times C(R_{\alpha\beta}, z_\alpha, z_\beta; [\rho_\alpha, \rho_\beta]). \quad (12)$$

In Eq. (12), $C(R_{\alpha\beta}, z_\alpha, z_\beta; [\rho_\alpha, \rho_\beta])$ is the direct correlation function in the liquid-vapor interface; it is a function of the relative locations of atoms of species α and β and of the densities of those species at the points. Equation (12) shows that, at the same temperature, the difference between the surface tensions of a pure liquid of species α and of the dilute alloy of β in α with β segregated in the liquid-vapor interface can only arise from differences between the longitudinal density gradients and between the direct correlation functions in the two liquid-vapor interfaces. These differences must be accounted for over the entire domain that the longitudinal density gradients are nonzero, which is typically three to four atomic layers for a liquid metal. Just as the qualitative difference between the structures of 2D and 3D solids leads to the expectation that the mechanisms by which these structures are brought about (crystallization) or destroyed (melting) will differ substantially, we must expect that the differences between quasi-2D and true 2D systems will have some signature in the phase diagram and the melting process.

With these caveats in mind, we now examine what general conclusions can be inferred from our calculations and from the experimental observations concerning the in-plane structure of the liquid-vapor interface of the dilute Pb in Ga alloy. The simplest situation would arise if the only effect of the substrate on the properties of the segregated monolayer in the liquid-vapor interface were to change the values of parameters that can be used in a 2D representation of it. The most renowned theoretical framework for 2D melting, the KTHNY formalism [17–20], describes melting as a two-stage process that proceeds via formation of an intermediate hexatic phase. The first transition, which is driven by spontaneous unbinding of the dislocations pairs to produce a "gas" of free dislocations, transforms the system from a solid to a hexatic phase. The latter phase lacks translational order but has quasi-long-range bond orientation order. In the following transformation dislocations dissociate further to form free disclinations, converting the hexatic phase into a fully disordered fluid. The KTHNY theory [17–20] predicts both transitions to be continuous, albeit it does not stipulate this to be the only possibility. As formulated, the KTHNY theory can be applied to any system that can be approximated as a continuous 2D elastic medium, regardless of the form of the potential energy function. We remark here that the KTHNY approach [17–20] to 2D melting identifies the transition with the limit of mechanical stability of the solid. The theory does not include any description of the liquid state and does not address any possible difference between the limit of mechanical stability and the limit of thermodynamic stability; the latter defines the melting point as the temperature and pressure at which the chemical potentials of the solid and liquid phases are equal. Our examination of the Q2D and 2D single-layer models of Pb shows that the character of the melting transition can be changed by out-of-plane motion of the Pb atoms. When out-of-plane motion is allowed the melting transition is first order and direct; i.e., a hexatic phase does not intervene between the solid and liquid phases. When out-of-plane motion is prohibited the melting transition the transition between the ordered solid and the disordered high-temperature phase appears to be continuous over a small but nonzero temperature range (see Figs. 6 and 13) and a hexatic phase does appear between the solid and liquid phases. Our results differ from those reported by Chekmarev, Oxtoby, and Rice [4]. An examination of their data shows that the conclusion that Q2D Pb layer melts first to a hexatic phase, then to a liquid phase, is based on very few points in the temperature dependence of the GOOP and GTOP. Given our experience that fluctuations near the melting temperature are persistent in the *NVT* ensemble simulations and that achievement of equilibrium in the transition region is very slow in a 2000-atom Q2D simulation sample, we believe that their simulations fell slightly short of achieving equilibrium.

It is worth noting that the effective atom-atom interaction derived from the pseudopotential representation is long ranged relative to the excluded volume interaction of hard spheres or the van der Waals interaction in simple liquids. Previously reported simulations of the mechanism of melting in 2D systems with long-range pair interactions have generated a variety of results. For example, Terao and Nakayama have reported the results of simulations of the behavior of a 2D assembly of charged colloidal particles at an air-water interface [23]. The interaction they use accounts for the dielectric properties of water, but the colloid motion is restricted to be strictly two-dimensional. The results obtained in these studies favor the KTHNY prediction of two-stage melting with continuous phase transitions. The molecular dynamics studies of a 2D classical electron system, by Muto

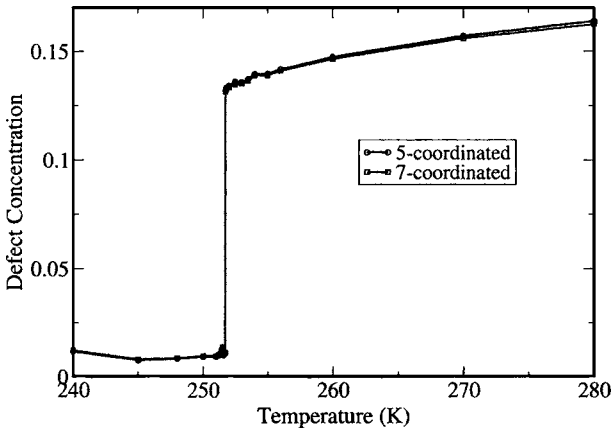

FIG. 25. The defect concentration in a Q2D Pb layer around its melting point. The concentrations of fivefold-coordinated and sevenfold-coordinated defects are almost identical, unless the temperature is much higher than the melting point.

and Aoki, suggests that the hexatic phase may, in fact, intervene between the stable solid and liquid phases, but no definitive statement concerning the order of the observed transitions was put forward in this work [24]. It should be noted that the use of a continuous rigid positive background to achieve charge neutrality in the system forces the transition to occur with zero change in density, a constraint that may affect the character of the phase transition.

We consider now the character and distribution of defects as the solid-to-liquid phase transition is traversed. As in our previous work, we have followed the conventional procedure of identifying defects via the Voronoi polygon mapping of the atom spatial configuration. A defect is defined to be an atom with other than six nearest neighbors; these are mapped as Voronoi polygons with other than six sides. Sevenfold and fivefold Voronoi polygons are classified as free disclinations. A bound pair of sevenfold and fivefold defects is a dislocation. At any nonzero temperature the Q2D solid has a small concentration of bound pairs of dislocations (quartets of disclinations), but their presence does not disrupt the quasi-long-range translational order. Just below the melting point of the Q2D system there are also clusters of bound pairs of dislocations. At any given temperature in the stable domain of the Q2D solid, defects with different coordination numbers—say, 4 and 8—have significantly smaller concentrations than the defects already mentioned. Consequently, they are assumed to play a minor role in defining the melting process. The concentrations of fivefold-coordinated and sevenfold-coordinated atoms found in our Q2D simulation sample, as a function of temperature, are shown in Fig. 25. There is an obvious discontinuity in the concentrations of these defects at the first-order melting transition. The concentration of the several species of defects and snapshots of several defect distributions are shown in Figs. 26 and 27.

Turning now to the PbGa bilayer, we show in Figs. 28–30, respectively, the concentrations of fivefold- and sevenfold-coordinated atoms, the composition of the defects by species, and snapshots of several defect distributions at different temperatures. Clearly, the rise in defect concentration with increasing temperature calculated in the bilayer system is not as steep as in the monolayer system. The defect concentration of the Pb layer of the bilayer shows steps at the

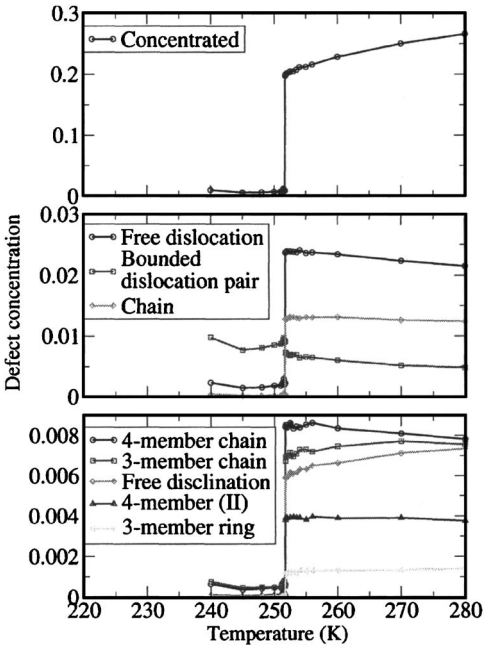

FIG. 26. The concentrations of the several species of defects of a Q2D Pb layer around its melting point. The four-member (II) notation means that three defects are neighbors to each other, while the fourth defect is a neighbor to only one of them.

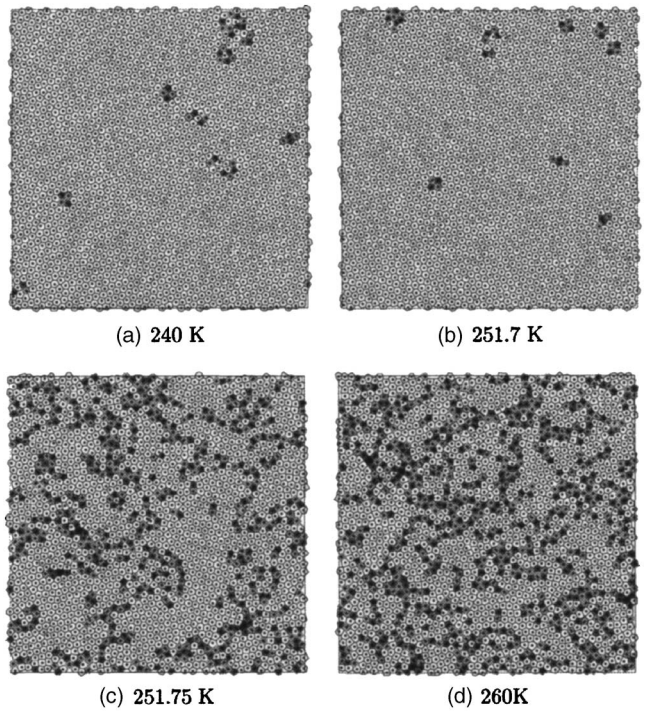

FIG. 27. Several sample configurations of a Q2D Pb layer. Voronoi polygons are shown. Defects are labeled as colored polygons; fivefold- and sevenfold-coordinated defects are shown as red and green, respectively; fourfold- and eightfold-coordinated defects are usually much lower in concentration and are labeled, respectively, as yellow and blue.

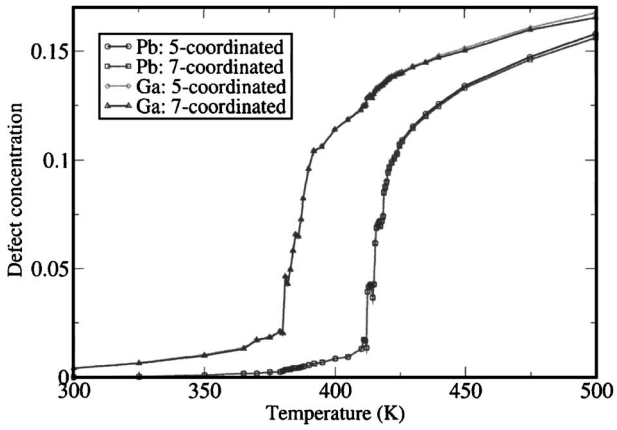

FIG. 28. The defect concentration in a PbGa bilayer. For each layer the concentrations of fivefold-coordinated and sevenfold-coordinated defects are very close to each other.

same temperatures that we identify with the Q2D crystal–to–hexatic-I and the hexatic-I–to–hexatic-II transitions. Despite the differences in the temperature profiles of the total defect concentrations in the one-layer and two-layer systems and the differences in the mechanism of melting, the composition of the defect populations in the two systems is very similar (compare Figs. 26 and 29).

Well below the melting temperature, the defect structure of the Q2D solid is consistent with the assumptions of the KTHNY theory [17–20]. In this temperature regime defects occur only in the form of tightly bound dislocation pairs and are present at very small concentrations. However, there appear to be many types of crystal defects that participate in the phase transition. At the melting transition temperature the total defect concentration increases discontinuously, and most defects are concentrated in clusters of various types. The concentrations of free dislocations and dislocation pairs are large, but the concentration of chains of dislocations is not much less than that of dislocation pairs. The range spanned by the concentrations of free disclinations and of various connected groups of three and four dislocations is less than a decade.

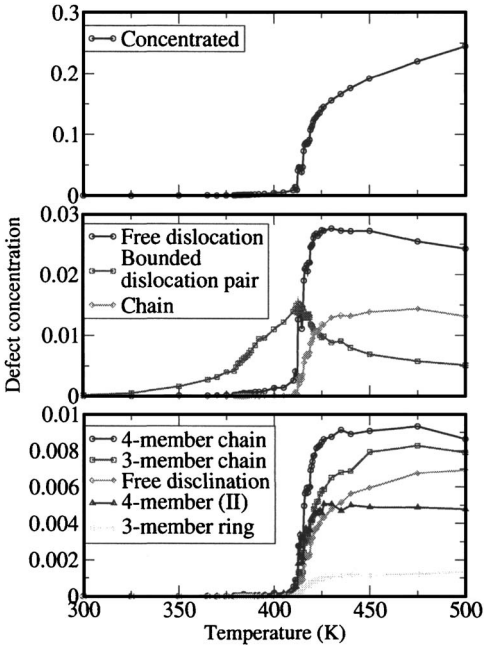

FIG. 29. The concentrations of the several species of defects of a PbGa bilayer around its melting point.

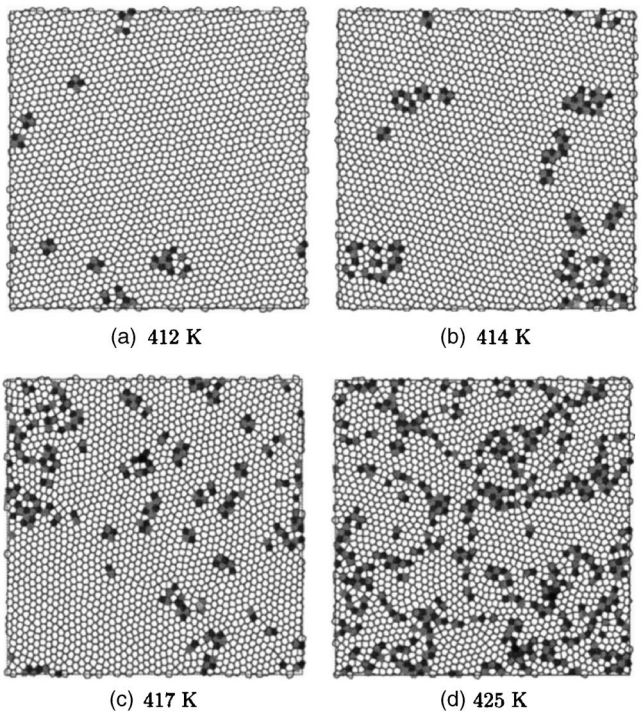

FIG. 30. Several sample configurations of a PbGa bilayer. Voronoi polygons are shown. Defects are labeled as colored polygons, in the same scheme as in Fig. 27. (a) shows a typical crystalline structure at a temperature just below the melting point; (b) and (c) show typical configurations for the hexatic (I) and (II) phases, respectively; (d) shows a typical liquid configuration.

Overall, the results of our simulation studies establish that the structures and the character of the phase transitions supported by a segregated monolayer in the liquid-vapor interface of a dilute alloy have strong dependencies on both the out-of-plane motion of the monolayer and its interactions with the substrate. A realistic picture of the behavior of that monolayer cannot be obtained from strictly two-dimensional models.

ACKNOWLEDGMENT

This research was supported by a grant from the National Science Foundation.

APPENDIX

In addition to the *NpT* ensemble simulations described in the text we also carried out *NVT* ensemble simulations for the same model systems. Indeed, we first chose to use the

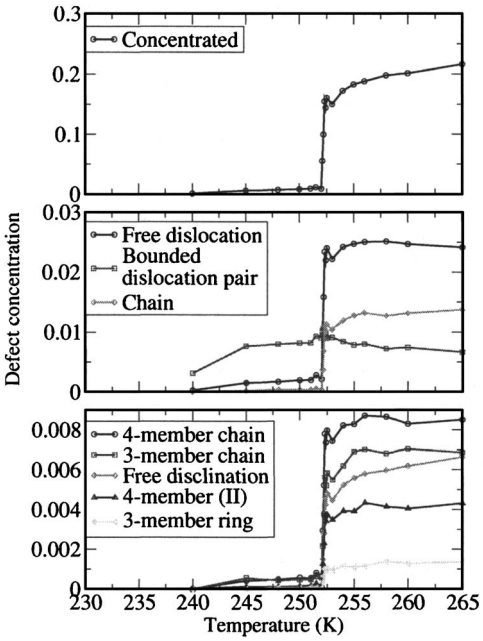

FIG. 31. The concentrations of the several species of defects of a Q2D Pb layer around its melting point, calculated in *NVT* ensembles.

NVT ensemble because the experimental data indicate that the change in density across the phase transition observed in the Pb monolayer is very small or zero. Moreover, simulations in the *NVT* ensemble are much faster than simulations in the *NpT* ensemble because, in the latter, the neighbor list used for computing interactions must be reconstructed after an accepted surface area change. However, near the transition temperature we found it harder to equilibrate the system in the *NVT* ensemble than in the *NpT* ensemble. Nevertheless, the results obtained from *NVT* ensemble simulations are sensibly identical with those obtained from the *NpT* ensemble simulations. It is illustrative to compare the results from the *NVT* ensemble simulations with those from the *NpT* ensemble simulations, which we do briefly in this appendix.

As in the text, we consider first the results obtained from *NVT* ensemble simulations of the Pb monolayer. The order parameters at temperatures around the transition point are displayed in Fig. 12. The transition temperature is found to be between 252.2 and 252.3 K. There are very dramatic changes in both order parameters at the transition temperature, but these changes are not as apparently discontinuous as found in *NpT* ensemble simulations. We attribute the difference to the fact that in the *NVT* ensemble, at temperatures just above the transition temperature, the Pb monolayer fluctuates between the ordered and disordered structures. Immediately above the transition temperature the global orientation order parameter is greater than the global translational order parameter. The GOOP then decays to be nearly equal to the GTOP over a range of about 5 K. This is basically the same behavior as was found in the *NpT* ensemble simulations, but the residual magnitude of the GOOP immediately after the transition is greater in the *NVT* ensemble. Figure 31 displays the concentrations of different defects in the Pb monolayer as a function of temperature. Clearly, the behavior

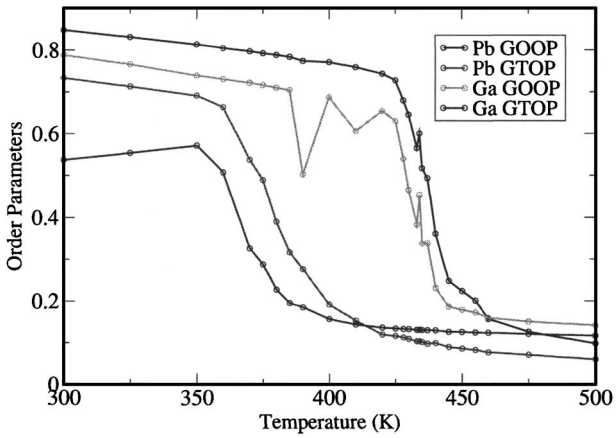

FIG. 32. The order parameters of a PbGa layer, calculated in *NVT* ensembles. Lines are shown to guide the eye.

illustrated in Fig. 30 resembles that shown in Fig. 26. These results show that, despite the constant density constraint in the *NVT* ensemble calculations, the melting mechanism is the same in the *NpT* and *NVT* ensembles.

Consider, now, the *NVT* ensemble simulations of the PbGa bilayer. The variations of the order parameters GOOP and GTOP with temperature are displayed in Fig. 32. There are dramatic changes in the GOOP and GTOP in a small range of temperature, but these changes are less like a discontinuous change than the comparable changes displayed in Fig. 15 for the *NpT* ensemble. We suggest that this disagreement is an artifact arising from the large structural fluctuations in the *NVT* ensemble near the transition temperature. In turn, we expect that artifact to disappear as the simulation

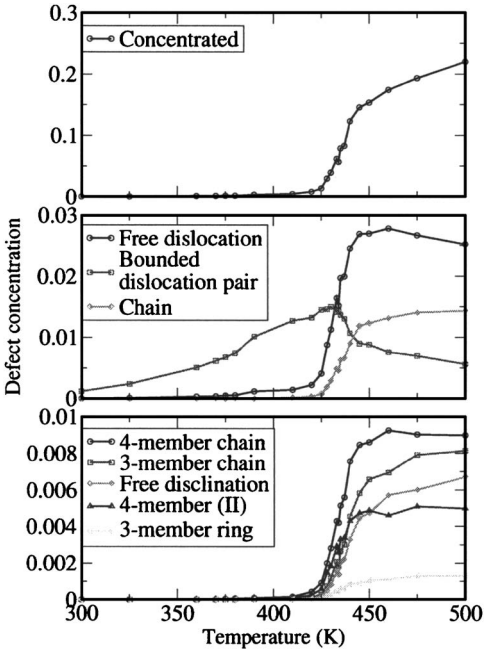

FIG. 33. The concentrations of the several species of defects of a PbGa bilayer around its melting point, calculated in *NVT* ensembles.

sample size is increased. Finally, we display in Fig. 33 the concentrations of various defects in the Pb monolayer. Clearly the several defect concentrations depend on the temperature in broadly the same way in both ensembles (see Fig. 29). Just as was the case for the GOOP and GTOP temperature dependences, the changes in the vicinity of the transition temperature are less abrupt in the *NVT* ensemble than in the *NpT* ensemble.

[1] B. Yang, D. Li, and S. A. Rice, Phys. Rev. B **62**, 13111 (2000).
[2] D. Li, X. Jiang, B. Yang, and S. A. Rice, J. Chem. Phys. **122**, 224702 (2005).
[3] M. Zhao and S. A. Rice, Phys. Rev. B **63**, 085409 (2001).
[4] D. S. Chekmarev, D. W. Oxtoby, and S. A. Rice, Phys. Rev. E **63**, 051502 (2001).
[5] M. Zhao, D. S. Checkmarev, Z.-H. Cai, and S. A. Rice, Phys. Rev. E **56**, 7033 (1997).
[6] C. H. Woo, S. Wang, and M. Matsuura, J. Phys. F: Met. Phys. **5**, 1836 (1975).
[7] M. Matsuura, C. H. Woo, and S. Wang, J. Phys. F: Met. Phys. **5**, 1849 (1975).
[8] R. W. Shaw, J. Phys. C **2**, 2335 (1969).
[9] M. P. D'Evelyn and S. A. Rice, J. Chem. Phys. **78**, 5225 (1983).
[10] A. A. Abrahamson, Phys. Rev. **178**, 76 (1969).
[11] J. O'Rourke, *Computational Geometry in C* (Cambridge University Press, London, 1998).
[12] D. R. Nelson, in *Phase Transitions and Critical Phenomena*, edited by C. Domb and J. L. Lebowitz (Academic, London, 1983), Vol. 7.
[13] M. A. Glaser and N. A. Clark, Adv. Chem. Phys. **83**, 543 (1993).
[14] J.-P. Hansen and L. Verlet, Phys. Rev. **184**, 151 (1969).
[15] D. G. Grier and C. A. Murray, in *Ordering and Phase Transitions in Colloidal Systems*, edited by A. K. Arora (VCH, New York, 1995).
[16] G. Aeppli and R. Bruinsma, Phys. Rev. Lett. **53**, 2133 (1984).
[17] J. M. Kosterlitz and D. J. Thouless, J. Phys. C **5**, L124 (1972).
[18] B. I. Halperin and D. R. Nelson, Phys. Rev. Lett. **41**, 121 (1978).
[19] D. R. Nelson and B. I. Halperin, Phys. Rev. B **19**, 2457 (1979).
[20] A. P. Young, Phys. Rev. B **19**, 1855 (1979).
[21] K. Chen, T. Kaplan, and M. Mostoller, Phys. Rev. Lett. **74**, 4019 (1995).
[22] D. G. Triezenberg and R. Zwanzig, Phys. Rev. Lett. **28**, 1183 (1972).
[23] T. Terao and T. Nakayama, Phys. Rev. E **65**, 021405 (2002).
[24] S. Muto and H. Aoki, Phys. Rev. B **59**, 14911 (1999).